Spectrochimica Acta Part B: Atomic Spectroscopy 200 (2023) 106589

Contents lists available at ScienceDirect

Spectrochimica Acta Part B: Atomic Spectroscopy

journal homepage: www.elsevier.com/locate/sab

Investigation on plasma enhanced decomposition of ammonium dinitramide (ADN) based propellant with optical diagnosis

Fangyi Wang [a,b], Shaohua Zhang [a,*], Xilong Yu [a,b]

[a] State Key Laboratory of High Temperature Gas Dynamics, Institute of Mechanics, Chinese Academy of Sciences, Beijing 100190, China
[b] School of Engineering Science, University of Chinese Academy of Sciences, Beijing 100049, China

ARTICLE INFO

Keywords:
Optical emission spectroscopy
Glow to filamentary discharge transition
ADN-based propellant
Plasma parameter

ABSTRACT

Plasma-enhanced decomposition is a promising method to achieve reliable ignition and better thruster performance with an ADN-based propellant. High-speed imaging and optical emission spectroscopy are used to characterize the discharge plasma produced from ADN-based propellant vapor and argon carrier gas within parallel planes. Discharge regimes are independently controlled by varying working parameters. The transition from abnormal glow discharge (AGD) to filamentary discharge (FD) is identified from voltage-current characteristics and sudden changes in excitation electron temperature ($T_{e\text{-}exc}$) and electron density (N_e) under a pressure of 0.2–10 kPa. Instabilities develop because there are more freedom degrees and higher collision probabilities after ADN-based propellant vapor is added. The product of $T_{e\text{-}exc}$ and N_e shows a higher energy transfer efficiency from input power to vapor in the FD regime. Water molecules increase the net dissociative attachment rate and effectively quench N_e. Although preheated vapor (as the discharge medium) has a much lower N_e, more radicals appear such as OH, NH, CH, CN, N_2, N_2^+, and C_2, which promote chemical interactions in an electric field and increase the probability of successful ignition. This can be attributed to thermalization due to an increase in the translational kinetic energy and rotational excitation, which has an important impact on chemical reaction kinetics. Therefore, preheating is verified as critical for improving the ignition and performance of a plasma-assisted ADN-based thruster.

1. Introduction

Hydrazine is a state-of-the-art liquid monopropellant for chemical space propulsion but has the disadvantages of high toxicity and higher overall cost. To reduce environmental and human health hazards, the concept of a "green" monopropellant has been proposed and some energetic ionic liquids studied. As potential alternatives to hydrazine, ADN-based liquid monopropellants have been studied since the 1990s because of their lower toxicity and vapor pressure [1], which make them easier and safer to handle. Such mixtures usually contain ADN as an oxidizer, fuel such as methanol or methylamine nitrate, and a solvent such as water. A typical ADN-based propellant is LMP-103S, with a formulation of 63.4% ADN, 11.2% methanol (CH_3OH) and 25.4% water (H_2O). LMP-103S produces environmental-friendly exhaust species (H_2O, N_2, H_2, CO, CO_2) after complete combustion.

Fig. 1 shows the reaction paths of an ADN-based propellant that uses CH_3OH as fuel. With an alterable formulation, an ADN-based propellant offers an adjustable specific impulse and combustion rate. The conventional way to ignite a propulsion thruster based on an ADN-based propellant is catalytic ignition, which uses a preheated solid catalyst. However, the fatal problem during catalytic ignition is that the solid catalyst is sintered, reduced, and deactivated when the combustion temperature reaches several thousand kelvins (i.e., adiabatic flame temperature) [2]. Therefore, researchers have been exploring many other ignition methods such as laser ignition, thermal ignition, and torch ignition to solve the problem and improve the performance of ionic liquid-based propulsive system. A possible way to solve the problem above is using a manageable ignition method. Non-equilibrium plasma has shown high potential in plasma-assisted ignition/combustion in recent years [3–5]. Specifically, discharge plasma is expected to enhance ignition and combustion through radical reactions and intense electric fields because it contains many excited species. Adding plasma to a reaction system also causes electro-thermal acceleration of reacting gases, which increases the propulsive efficiency.

Apart from the coupling enhancement by the plasma, the complex physico-chemical properties of an ADN-based propellant also introduce

* Corresponding author.
E-mail address: shzh@imech.ac.cn (S. Zhang).

https://doi.org/10.1016/j.sab.2022.106589
Received 1 July 2022; Received in revised form 15 November 2022; Accepted 23 November 2022
Available online 30 November 2022

fundamental challenges that have prevented full evaluation of the interactions between the mixed propellant and discharge plasma. Quantitative insight into the discharge process of an ADN-based propellant is still lacking owing to the poor understanding of plasma instability in the vapor phase, molecular ionization, and chemical reactions that produce radicals and charge transport. Therefore, it is vital to explore and create related bench experiments not only to compensate for the relative scarcity of experimental data, but to lay the foundation for measuring ignition and combustion characteristics of plasma-assisted ADN-based thrusters.

Optical emission spectroscopy (OES) is often used to investigate plasma [6] by detecting spectral radiation owing to its non-intrusiveness and traceability. Many studies use water when applying and developing OES in vapor [7,8] and liquid phase [9–11]. For example, Clements et al. observed through OES that radical density increased greatly when gas was bubbled through a hollow high-voltage electrode directly inside water [12]. However, there are hardly any experimental reports showing how an ADN-based propellant is involved with electron density and electron excitation temperature during the interactions.

One of the difficulties in quantitative bench studies is mixing the gas of interest and the ADN-based propellant vapor in a uniform flow field. The approach used in this work is to draw from a sampling bottle to introduce the vapor into the measurable flow field through a carrier gas. The sampling bottle, which contains the ADN-based propellant, is placed in an oil bath, and the mass flow rate and vapor temperature variation are achieved by heating the oil inside. Considering the oxidizer inside the propellant, we select argon gas to avoid the coupling interaction during this initial exploration.

When the research shifts from fundamentals to applications, it is important to investigate a real industrial environment. To simulate an aero-propulsive environment, this work focuses on the pressure range 0.2–10 kPa. Plasma is produced by a sinusoidal alternating current (AC) power supply with an input power of 0–30 W considering the volume and weight limitations of an ADN-based thruster.

In this paper, plasma interacting with an ADN-based propellant is investigated using high-speed imaging and OES to measure basic plasma parameters including the discharge morphology, excitation electron temperature ($T_{e\text{-}exc}$), and electron density (N_e). Different products are found in the OES spectra under selected working conditions, and discharge plasma-assisted ADN-based propellant decomposition is verified by the spectra. $T_{e\text{-}exc}$ and N_e, which are calculated from the Boltzmann slope and Stark broadening, respectively, are used to quantitatively determine the plasma state. Further, the discharge regime transition is observed under the given pressure and input power, and the dominant instabilities during regime transitions are demonstrated. Finally, the impact of an ADN-based propellant on regime transition is analyzed in the discussion section. In brief, a critical investigation and real-time, in situ diagnosis is carried out to achieve external control of regime transition and enhance plasma. Additionally, characterizing plasma makes it easier to validate kinetic models [13] that involve ADN-based propellants and assess their predictive capability.

The discharge chamber used in this work has been described before [14], so only some important parameters are repeated here. A typical parallel copper plane configuration was used, as shown in Fig. 2. Each plane had a 15-mm square discharge area exposed. The distance between the two electrodes was 14 mm. The electrodes were inserted into a constant-volume tetrahedral chamber equipped with fused quartz windows on all four sides. Plasma was produced by a sine-wave high-voltage power supply (Coronalab CTP-2000 K, Nanjing, CN) with a frequency of 5 kHz, which is highly reproducible for shot-to-shot discharge. The input power was measured with high-voltage current probes connected to an oscilloscope.

Pure argon (99.999%) with a steady flow rate of 200 sccm (standard cm^3/min) was introduced into the chamber and monitored with a flow controller (CS200, SevenStar). A 75-mL Teflon sampler containing the ADN-based propellant was placed in an oil bath with dimenthyl silicone oil that could be heated to 300 °C. The argon was either introduced into the chamber only or into the sampler to produce a mixture composed of the ADN-based propellant and argon. The composition of this propellant was 63% ADN, 11% CH_3OH, and 26% H_2O (volume fraction). The mass flow of the propellant was controlled via the oil bath temperature. A stable chamber pressure was achieved by precisely adjusting the inlet and evacuation and monitored with a high-precision pressure sensor. Because the propellant needed to be preheated in working conditions, a translucent Teflon pipe with a thermal insulation belt in the exterior shell was used at the chamber entrance to avoid condensation. The propellant temperature was measured with a built-in thermometer in the sampler, and the propellant mass flow rate was obtained via the weight method [15].

Discharge images were captured through an optical window by a high-speed camera (FastCam SA-Z, Photron), which was placed directly in front of the electrodes. A lens was placed in front of the camera, and acquired images were displayed by a computer. A frame rate of 40,000 fps and exposure of 20 μs were set to visualize discharge evolution, so eight images were obtained during one sinusoidal period of the 5-kHz power supply. Experimental synchronization was controlled through a multi-channel digital delay pulse generator (DG645, Stanford Research System).

OES was carried out with a fiber-based spectrometer (Spectropro HRS-500, Princeton Instruments). This spectrometer had a grating with 1200 grooves/mm and a blaze wavelength of 500 nm. An optical fiber was positioned at the outer surface of a side optical window. This fiber

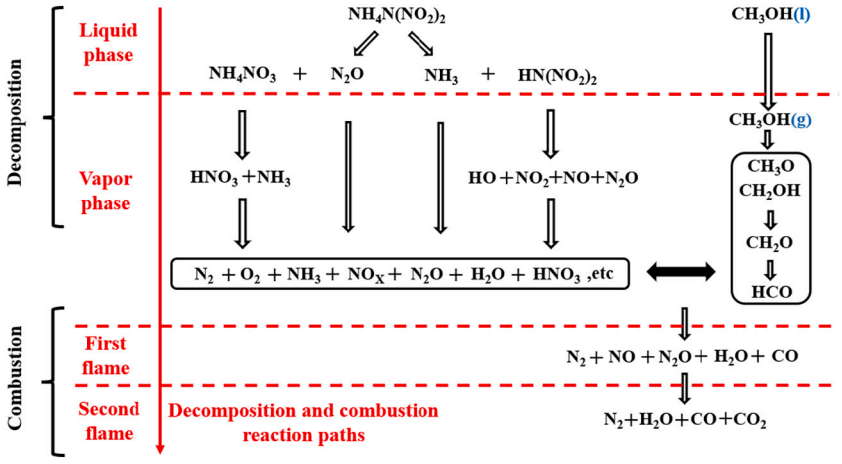

Fig. 1. Decomposition and combustion of an ADN-based propellant using CH_3OH as fuel.

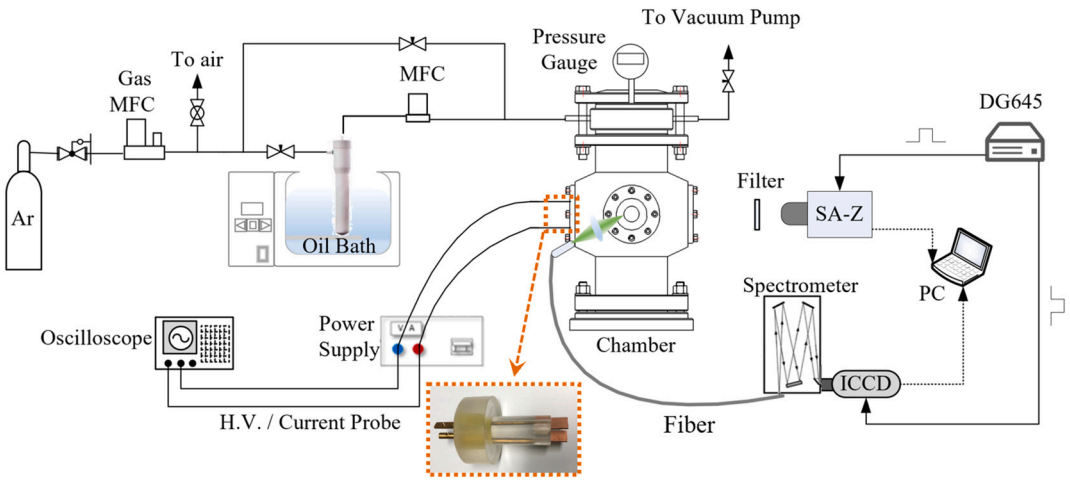

Fig. 2. Schematic of the experimental setup. 2. Experimental apparatus.

had a circular collection area of 1 mm^2 and was sealed in a ferrule head with a 10-mm diameter. The plasma signal was focused into the fiber by a quartz crystal with a focal length of 30 mm, and transmitted into the spectrometer through a 30-μm slit. Through this spectrometer, the signal went to an ICCD sensor (PI-MAX4, Princeton Instruments) whose gate width was set to 200 μs with an accumulation of five times during the experiment. The signal was averaged from three repetitions for a better signal-to-noise ratio (SNR). The grating efficiency of the spectrometer was calibrated with a standard tungsten halogen lamp (63,976, Oriel Instruments), while the system wavelength was corrected with a standard Hg—Ar lamp.

Three working conditions were selected to study the plasma and its interaction with the propellant: Ar, Ar/ADN-based propellant with a mass flow of 0.25 g/h at room temperature (hereafter referred to as Ar + ADN), and Ar/heated ADN-based propellant with a mass flow of 0.79 g/h at a temperature of 323 K (hereafter referred to as Ar + preheated ADN).

2. Results and discussion

2.1. Typical spectra

The discharge products for different inlet substances were determined and the energy transfer mechanisms inferred from three typical spectra in the range 200–900 nm with a gas pressure of 400 Pa, as shown in Fig. 3. Fig. 3(a) shows the spectral lines of atomic and ionic argon and atomic copper.

In Fig. 3(b), the whole relative intensity of ionic argon lines (Ar-II) increases while the intensities of atomic argon (Ar—I) and copper (Cu—I from the electrodes) decrease when the argon gas goes through the sampler containing the ADN-based propellant at the room temperature of 293 K. The decrease in Ar—I intensity and increase in Ar-II intensity with higher ADN vapor content is mainly due to the change in mechanism of discharge energy transfer, it seems ADN vapor has promoted Ar ionization. The proportion of H atoms increases likely owing to the decomposition of N—H in NH_4^+ from ADN molecules because N—H has a much higher concentration and a lower bond energy (391 kJ/mol):

$$e^- + NH_4^+ \rightarrow NH_3 + H$$

Furthermore, OH radicals have a higher probability of coming from direct ionization, whereby the C—O bond in CH_3OH breaks (358 kJ/mol) and so does the H—O bond in H_2O (467 kJ/mol):

$$e^- + CH_3OH \rightarrow e^- + CH_3 + OH$$

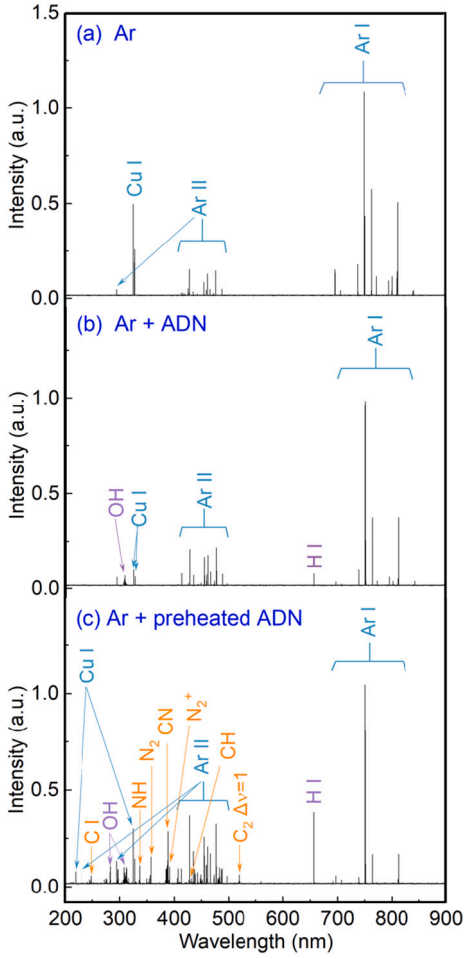

Fig. 3. Typical spectra of (a) Ar, (b) the Ar/ADN-based propellant, and (c) the Ar/heated ADN-based propellant with a gas pressure of 400 Pa.

$$e^- + H_2O \rightarrow e^- + H + OH$$

Generally, it is possible to precisely determine T_{rot} for OH radicals (309 nm $A^2\Sigma^+ \rightarrow X^2\Pi$) through fitting [16,17]. Unfortunately, the experimental OH spectrum has a low resolution that is difficult to distinguish from the base line. Direct electron excitation could achieve the transition energies needed to excite different species, and we

conclude that direct electron excitation rather than recombination is the main mechanism for emitting excited species.

Preheated vapor has higher vibrational, rotational, and translational kinetic energies as well as chemical reactivity owing to thermal energy conversion, which means the collision probability increases to produce more ions, radicals, and other excited species. Adding ADN vapor to the Ar gas discharge changes the rate of energy transfer between electrons and molecules. From the kinetic enhancement viewpoint, high-energy electron and ion production during discharge leads to production of active radicals via direct electron impact dissociation, ion impact, recombination dissociation, and collisional dissociation of reactants reacting with electronically excited and vibrationally excited molecules. Input thermal energy is partly converted to the intrinsic energy of the discharge medium and is usually used for rotational excitation; hence, the excited species more easily achieve the reactions above. As expected, more species of spectral lines appear when the ADN-based propellant is preheated to 323 K. Several new atoms, ions, and radicals are observed such as carbon atoms (247.8 nm), N_2 (357.7 nm, $C^3\Pi_u \rightarrow XB^3\Pi_g$), N_2^+ (391.4 nm, $B^2\Sigma_u^+ \rightarrow X^2\Sigma_g^+$), C_2 swan (516.3 nm, $D^3\Pi_g \rightarrow A^3\Pi_u$), NH (336 nm, $A^3\Pi \rightarrow X^3\Sigma$), CH (431 nm, $A^2\Delta \rightarrow X^2\Pi$), and CN radicals (388 nm, $B^2\Sigma^+ \rightarrow X^2\Sigma^+$). The CN radicals are from ion irradiation of the vapor and chemical interactions, where C is from the fuel CH_3OH and N is from the oxidizer $NH_4N(NO_2)_2$. There is a more obvious variation in relative intensity of spectral lines in Fig. 3(c). The spectral lines of Ar—I at 772.4 nm, 794.8 nm, and 801.4 nm cannot be distinguished from the background signal, which indicates a greater reduction in Ar—I intensity. Meanwhile, both the intensity and number of Ar-II lines increase from Fig. 3(a) to Fig. 3(c). This is because the mechanism of discharge energy transfer changes after ADN vapor is added to the discharge medium.

The dominant discharge mechanism in low-pressure cases is secondary electron emission. It seems the appearance of vapor in the discharge field promotes secondary electron emission and discharge performance, as demonstrated by the greater number of spectral lines. In addition, CH_3OH has been shown to interact with ADN at the middle and downstream positions inside an engine with traditional catalytic ignition [5]. However, the generation of C_2* free radicals indicates that preheated CH_3OH dissociates when it is exposed to the discharge field. C_2* free radicals may be produced by direct reaction of groups containing multiple carbon atoms with other groups or enhanced saturated hydrocarbon molucules undergo a dehydrogenation reaction. We infer that CH_3OH performs better during oxidation to produce CO or CO_2 when it interacts with plasma via reaction paths such as $C_2 + OH = CH^* + CO$. The appearance of N_2 implies an ADN dissociation path such as $ADN \rightarrow N_2O + AN$, $N_2O \rightarrow 2N_2 + O_2$. This dissociation combined with CH_3OH oxidation has played a significant role in temperature steps during combustion [5]. In conclusion, discharge energy is used to dissociate Ar gas when there is only Ar in the chamber. Part of the discharge energy is used to produce OH radicals and H atoms after ADN vapor is introduced under room temperature. More radicals and chemical reactions appear with preheated ADN vapor because the mass flow rate and intrinsic energy have increased.

Pre-analyzing spectra is essential for identifying different substances and revealing energy transfer processes, especially for the vapor sample. Considering the electric field determines the various types of collisions that occur in plasma, it is necessary to investigate the electrical characteristics.

2.2. Regime transition

Most plasmas produced within vapors or in contact with vapors are highly transient, so different regimes appear when discharge parameters vary [18]. The relative importance of energy transfer mechanisms in various types of collisions depends on the electric field, which is characterized by electrical parameters. The input voltage–current curves were recorded on an oscilloscope. Fig. 4 shows the corresponding discharge phenomena captured by a high-speed camera. The illumination in the images represents the electron distribution while the color represents the electron number density to some extent. Electrons alternate on the electrode surfaces with a cycle determined by the frequency of the AC power supply. Regime transition changes the discharge morphology in some way. The abnormal glow discharge (AGD) only covers the electrode surfaces, and the filamentary discharge (FD) consists of luminous columns and is surrounded by a diffuse glow, as the images in Fig. 4 show. At first these columns are secondary avalanches

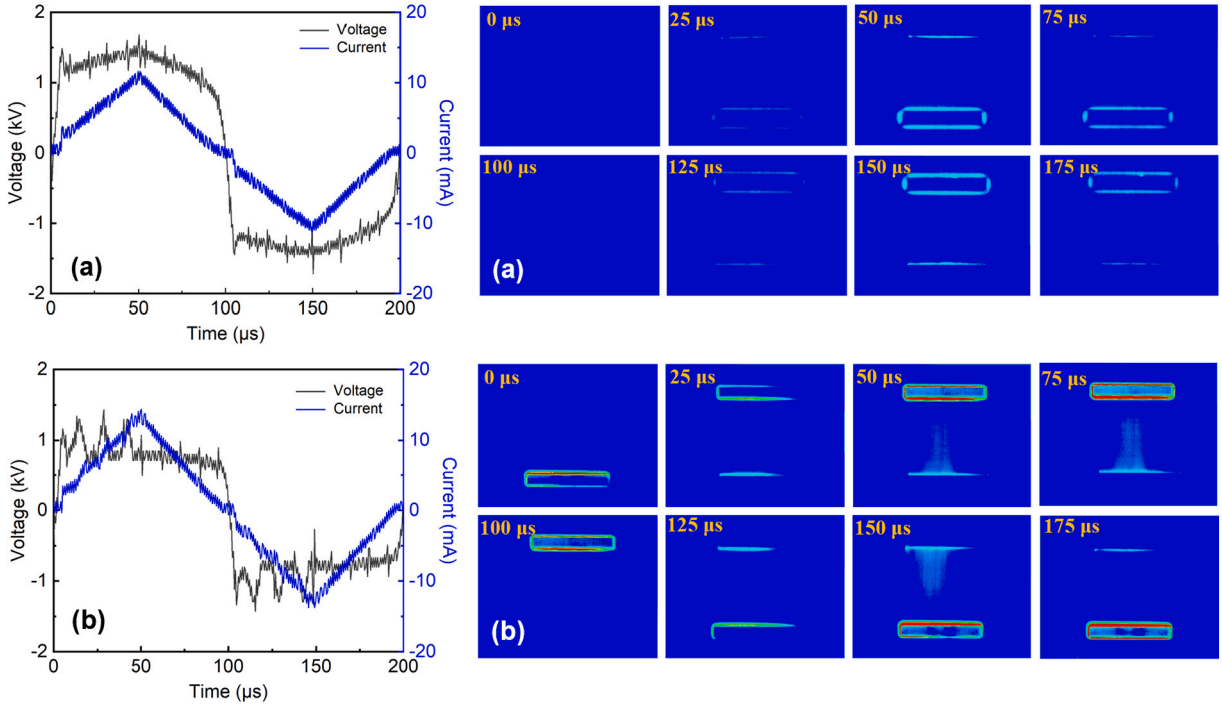

Fig. 4. Voltage–current curve and discharge images for (a) AGD at a pressure of 400 Pa and (b) FD at a pressure of 4 kPa.

initiated by photoionization and photoemission. They then tend to converge toward a local primary avalanche and develop into a highly conducting filamentary channel bridging the discharge gap that marks the transition from the AGD to the FD regime. In FD, distributed transient streamers randomly fill the space between electrodes because the seed electron density just before this breakdown is high enough (which is verified in Section 3.4). This leads to numerous small avalanches at the origin of the streamer formation, preventing further transition to arc discharge; that is, only one concentrated avalanche is produced. The voltage curve for FD oscillates more intensely than that of AGD, which is similar to the results of Bruggeman et al. [19]. Constriction during the transition may be affected by heat accumulation during AGD as we discussed in a previous study [14]. Owing to thermal instability, FD has a more unstable and pronounced oscillating voltage curve according to the regular voltage and current curves in Fig. 4. The discharge images also reflect the electron density to some extent. The reduction in apparent filament diameter could be due to the introduction of electronegative species (such as water vapor and oxygen) to the discharge mixture, or a lower voltage, or a locally nonuniform electric field distribution.

Estimating the filament diameter from the images in Fig. 4 allows us to determine the maximal electron concentration from the current density (peak value) if the electron mobility is known [20]:

$$J = N_e e v_e \left(\frac{E}{N}\right) = N_e e \mu_e E \tag{1}$$

where J is the current density, e is the elementary charge I/s, E is the electric field in V/m, and μ_e is the electron mobility in argon. According to the value of μ_e for multichannel surface glow discharge in pure argon in Ref. [21], $\mu_e p = 0.23 \times 10^6$ cm^{2}Torr/V s $\rightarrow \mu_e = 0.03$ m^2/V s. Therefore, when we assume the discharge object is just argon, N_e is estimated as 5.3×10^{14} cm^{-3} using Eq. (1). This will be discussed in detail in Section 3.4.

We analyze the transition from an abnormal glow breakdown to a filamentary breakdown on the basis of electrical parameters coupled with the visual discharge images. The voltage and current amplitudes are displayed in Fig. 5 to investigate individual trends as input power rises. Because the sustaining voltage increases in proportion to the current in Fig. 5(a), (c), (e), the glow discharge in this experiment is defined precisely as abnormal. As the input voltage increases in the AGD regime, the number and energy of positive ions on the cathode also increase. The resistance of the discharge gas decreases sharply once the cathode reaches a high temperature, and the discharge transitions from AGD to FD. Consequently, the voltage decreases with current in Fig. 5(b)(d)(f) because of the negative resistance of plasma. Note that regime transition did not happened within current input power range. Owing to the gas pressure has a main impact on regime transition compared with input power in this study, it is concluded that energy transfer mainly through collisions during the transition.

Compared with the regime transition (from AGD to FD) under a pressure range of 2–3 kPa in pure Ar, the transition in Ar + ADN and Ar + preheated ADN shifts to a smaller pressure range: 1–2 kPa. It seems the propellant vapor carried by Ar accelerates the regime transition, which is dominated by electron avalanches due to direct electron collisions as pressure increases. This leads to large local space charges and secondary avalanches propagating into the FD region. Furthermore, the heated propellant is a larger proportion of the total propellant under the same working pressure, there is a higher collision probability to produce more radicals from many molecules in propellant. Meanwhile, the internal energy of the vapor has increased because thermal energy is converted to either translational kinetic energy or rotational excitations. Durocher et.al's [22] work also implies that electron-impact dissociation reactions and energy transfer collisions from excited rotational states improve in an admixture of molecules as a result of neutral gas heating.

As Fig. 5(a)(b) shows, voltage increases as current rises in the AGD regime, while the FD regime has the opposite voltage–current characteristics. Plasma resistance decreases as gas pressure rises from 0.2 kPa to 2 kPa, and then increases from 3 kPa to 10 kPa. Adding ADN vapor under room temperature prompts electron multiplication as indicated by the lower resistance in the AGD regime. Preheated vapor with a temperature of 323 K further accelerates this effect, as evidenced by the lower voltage and higher current in Fig. 5(a)(c)(e). In the FD regime in Fig. 5(b)(c), the collision probability also increases a lot with preheated vapor, so the peak current increases. The input power is treated as an independent variable in the following sections because current and voltage both change along with the discharge settings.

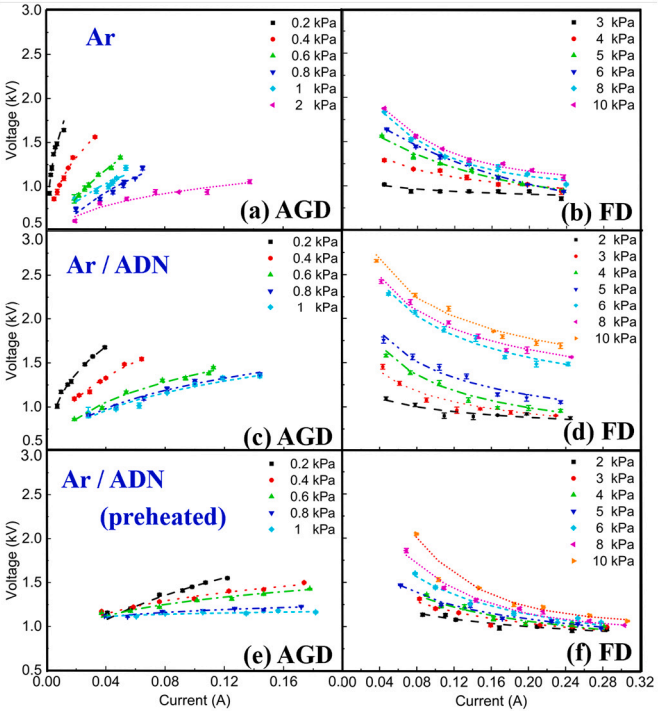

Fig. 5. Current and voltage amplitudes in (a)(b) Ar, (c)(d) Ar/ADN-based propellant, and (e)(f) Ar/heated ADN-based propellant for the (a)(c)(e) AGD regime and (b)(d)(f) FD regime.

2.3. Calculating plasma properties

As a characteristic parameter of the electron energy distribution function (EEDF), $T_{e\text{-}exc}$ represents most of the discharge energy emitted via radiative decay. The widely-used Boltzmann slope method is used to calculate $T_{e\text{-}exc}$, which requires the plasma to be at least in partial local thermal equilibrium (PLTE) [23,24]. This is possible if collisional ionizations and radiative recombinations dominate the discharge process. Furthermore, it still requires the system to be highly collisional with a high electron density, which is verified in the next section. Provided the plasma is in PLTE, $T_{e\text{-}exc}$ can be determined via

$$ln\left(\frac{I\lambda}{A_{ki}g_k}\right) = -\frac{E_k}{kT_{e-exc}} + C \tag{2}$$

where I is the relative spectral line intensity, λ is the wavelength, k is Boltzmann's constant, g_k and E_k are the statistical weight and the energy of the upper level respectively, and A_{ki} is the Einstein transition probability in Table 1. The six spectral lines of Ar—I in Table 1 are used to calculate $T_{e\text{-}exc}$ via the Boltzmann slope method.

Aside from the thermal effect, chemical chain reactions are also accelerated by charged active particles with low activation energy produced by collisions in the discharge gap. Excited species are produced from CH_3OH, H_2O, ADN molecules, and Ar gas. Accordingly,

Table 1
Spectroscopic data for argon used in OES.

Element	Wavelength	Absolute spontaneous transmission probabilities	Transition energy of upper levels	Statistical weight
	λ (nm)	A_{ki} ($10^6 s^{-1}$)	E_k (cm^{-1})	g_k
Ar-I	696.5431	6.4	107,496.4166	3
	706.7218	3.8	107,289.7001	5
	750.3868	45	108,722.6194	1
	751.4651	40	107,054.2720	1
	763.5106	24.5	106,237.5518	5
	811.5311	33	105,462.7596	7

ignition and combustion performance may improve significantly in the presence of even a small amount of free electrons. A higher value of N_e is expected to accelerate the reaction rate from the kinetic aspect. This can also be determined from the Stark broadening. The full width at half maximum (FWHM) of the chosen spectral lines can be obtained from Voigt fitting and instrumental broadening (measured with a standard Ne/Ar light source). Van der Waals broadening and natural broadening are removed to obtain Stark broadening. Hence, N_e is calculated from

$$\Delta\lambda_{stark} = 2\times\left[1+1.75\times10^{-4}N_e^{\frac{1}{4}}\alpha\times\left(1-0.068N_e^{\frac{1}{4}}T_e^{-\frac{1}{2}}\right)\right]\times10^{-16}\omega N_e \quad (3)$$

where α is the static ion-broadening parameter, and ω is the electron impact half-width [25]. We can use the criterion

$$N_e \geq 1.6\times10^{12}\sqrt{T}\,(\Delta E)^3 \quad (4)$$

from MCWHIRTER's work [26] to check the PLTE assumption. It can be shown that the measured plasma meets this criterion, which means it has reached the PLTE state.

2.4. Plasma properties in argon gas discharge

First, the PLTE assumption is proved with the criterion in Eq. (4) using the values of $T_{e\text{-}exc}$ and N_e obtained with the method described in the last section. With $T_{e\text{-}exc} < 8000$ K and $\Delta E \approx 1.78$ eV under all working conditions, the PLTE assumption is met when $N_e \geq 8.071\times10^{14}$ cm^{-3}.

Our previous study concluded that pressure has a larger influence on regime transitions when the input discharge power is in the range 0–25 W. In this work, we similarly investigate $T_{e\text{-}exc}$ and N_e under different input powers and pressures. As Fig. 6 shows, $T_{e\text{-}exc}$ and N_e have the same order when the pressure range is from 3 kPa to 10 kPa and the input power is below 20 W. Overall, considering the discharge energy balance, $T_{e\text{-}exc}$ decreases with input power while N_e increases when the discharge medium is only Ar. However, there is an opposite trend in $T_{e\text{-}exc}$ as a function of input power in the FD regime after ADN vapor is added to the discharge medium. This is due to the effect of the vapor on the local electric field, which implies a more efficient discharge energy conversion.

To discuss the regime transition process, we plot $T_{e\text{-}exc}$ and N_e in Fig. 7 for an input power of 5 W. Sudden changes in both parameters indicate that the regime has transformed from AGD to FD when the gas pressure is 2–3 kPa. From our previous conclusions, thermal instability plays a dominant role during the AGD-to-FD transition. A sudden rise in $T_{e\text{-}exc}$ is observed this time when there is a finer partition of the pressure interval, that is, more sampling points in the range 0.2–10 kPa. This confirms that the thermal instability is the main instability that leads the transition from AGD to FD with only argon as the medium.

Because the PLTE assumption has been verified, the electrons are regarded as being in local thermodynamic equilibrium, so the distribution function is supposed to be Maxwellian:

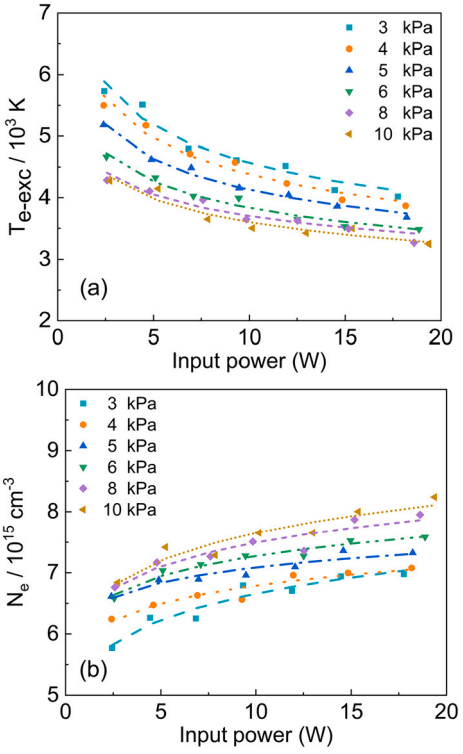

Fig. 6. Excitation electron temperature and (b) electron density during FD with only argon gas in the discharge chamber.

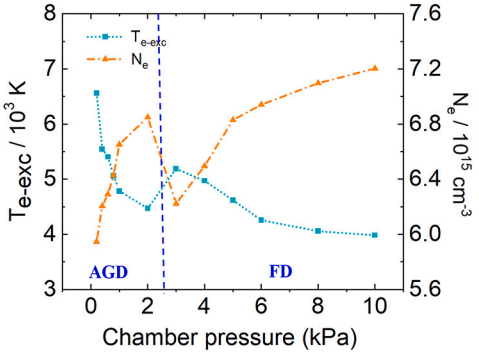

Fig. 7. Excitation electron temperature and electron density with only argon gas in the discharge chamber when the input power is 5 W.

$$f_E(E) = 2\sqrt{\frac{E}{\pi}}\left(\frac{1}{kT}\right)^{3/2} exp\left(-\frac{E}{kT}\right) \quad (5)$$

Thus, $T_{e\text{-}exc}$ in Fig. 7 can be used to determine the EEDF, which provides the electron elastic collision rates and inelastic processes such as ionization, excitation, and electron attachment. With higher chamber pressure in either the AGD or FD regime, the EEDF has a lower fraction of high-energy electrons owing to the collision loss. It seems relatively high-energy electrons switch to being low-energy electrons during the regime transition.

2.5. Plasma properties in argon gas with an ADN-based propellant discharge

For comparison, $T_{e\text{-}exc}$ and N_e are drawn in the same plot in Fig. 8. Although adding ADN vapor increases the probability of inelastic collisions between electrons and molecules, $T_{e\text{-}exc}$ increases by

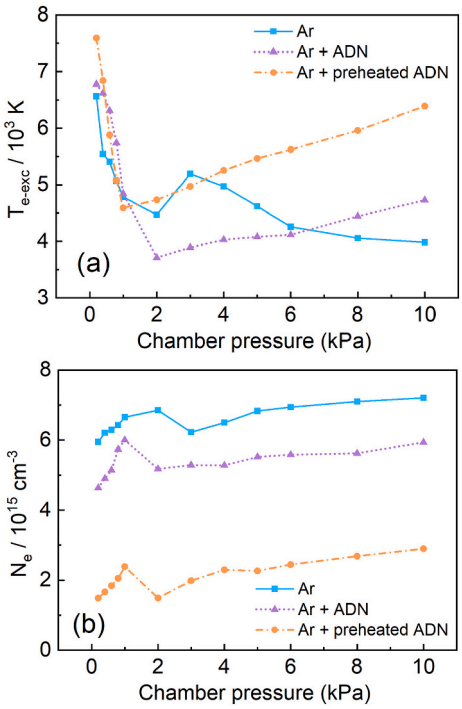

Fig. 8. (a) Excitation electron temperature and (b) electron density with three discharge mediums when the input power is 5 W.

approximately 15% from 0 to 1 kPa in the AGD regime compared with the pure-Ar case. In the AGD regime, almost all the discharge potential is concentrated in the narrow area near the cathode. As for the increase in Ar^+ intensity in Fig. 3, high-energy electrons collide with the ADN vapor molecules, producing OH and H spectral lines. In the FD regime (from 2 to 10 kPa), adding ADN vapor makes $T_{e\text{-}exc}$ rise but from a lower starting point. This is because the secondary electrons are "seeds" that have induced an avalanche that represents more electrons with low energy in the discharge field. In both the AGD and FD regimes, N_e from the Ar + ADN discharge medium decreases approximately 20% compared to the pure-Ar case. This is due to the inelastic collisions between electrons and molecules in one viewpoint. From another viewpoint, some studies [27–29] have reported that water can be a quencher in plasma. This means that part of the highly energetic electrons is dissociatively attached to H_2O molecules.

The discharge instability that leads to the regime transition after addition of ADN vapor to the medium occurs at a lower pressure according to the turning point in Fig. 8. It is difficult to distinguish whether thermal instability or electronic instability plays the leading role in the Ar + ADN case. However, when Ar and Ar + ADN are compared, the turning point in the $T_{e\text{-}exc}$ curve from 2 to 3 kPa to approximately 2 kPa and the sudden drop with N_e shift from 2 to 3 kPa to 1–2 kPa. Introducing ADN vapor to the discharge chamber increases the freedom degrees of plasma interactions and exacerbates the discharge instabilities.

Preheated ADN vapor represents a larger fraction of ADN at the same chamber pressure because of the higher propellant evaporation rate. Part of the discharge energy excites the large ADN molecules electronically and causes them to undergo dissociation (including dissociative attachment), as indicated by the appearance of NH, CH, OH, and N_2 spectral lines. Thermal energy from preheating has positive feedback on dissociation, so free radicals and ions have higher probabilities of colliding and recombining as new species such as C_2 and CN. Compared with the case of a pure-Ar medium in Fig. 8(a), the turning point has switched from 2 kPa to 1 kPa as a result of the thermal energy. $T_{e\text{-}exc}$ shows a minor difference in the AGD regime because it has a more stable discharge structure. In the FD regime, $T_{e\text{-}exc}$ increases by 25%, which suggests that ADN vapor in discharge channels works as an effective cathode electrode and the secondary electrons are emitted more efficiently than with metal electrodes [30]. Furthermore, the anode electrode (Cu plate) is bombarded by ions moving at a higher speed and sputtered Cu atoms because the local electric field changes. The momentum transfer from these collisions produces stronger atomic Cu spectral lines in Fig. 3(c). N_e during discharge in Ar + preheated ADN is reduced by a factor of approximately 3 compared with the Ar + ADN case. This is likely due to dissociative attachment to water vapor and more inelastic collisions of electrons with reactive particles. Above all, the CN spectral line implies some chemical reactions have already occurred inside the propellant. We infer that gas temperature (T_g) and N_e both decrease in the presence of ADN admixtures because of electron-impact dissociation reactions and energy transfer collisions in excited rotational states. In brief, thermal energy transfer to translational kinetic energy and excited rotational levels of $NH_4N(NO_2)_2$, CH_3OH, and H_2O through electron-impact excitation appears to be a key mechanism for plasma-assisted ADN vapor ignition or combustion over the range of experimental conditions investigated in this paper.

It is worth noting that ADN-based propellants have a strong background in engineering application. A benchmark should be determined for different engineering purposes. Wada et,al. [3] emphasize N_e for ADN-based thrusters during plasma-assisted ignition/combustion. Both $T_{e\text{-}exc}$ and N_e increase in FD regimes and reach maximum values at 10 kPa, which indicates a higher discharge energy efficiency when ADN vapor is added to the discharge field. Hence, appropriate working conditions should be selected when this is extended to thruster applications with different priorities.

Because regime transition is affected by the amount of ADN vapor and electron properties, the circuit impedance should be increased to control regime transition in further work. Current diagnosis should be improved with high spatio-temporal resolution to attain thorough understanding of electron transport and related electron kinetics in non-equilibrium plasma. Water is a very effective quencher for N_e, and should be removed or reduced by preheating, adjusting the composition of the ADN-based propellant, or other ways before plasma reactions.

3. Conclusion

Plasma-assisted ADN-based liquid propellant ignition/combustion is multi-faceted owing to the various kinds of chemical species decomposed from this mixture. Electrons, ions, radicals, and reactive species are involved in the electric field, and reactions in the discharge gap are related to the local heating and flow field. This paper has provided new high-speed images and OES data concerning plasma properties with Ar and ADN-based propellant vapor as discharge mediums. When ADN-based propellant vapor is added at a mass flow rate of 0.25 g/h, the spectral line intensity of Ar—I decreases and that of Ar-II increases, and H atoms and OH radicals appear. CH, NH, N_2, N_2^+, C_2, and CN radicals and ions are observed with preheated ADN-based propellant, suggesting that preheating significantly improves the performance of plasma-assisted ADN-based propellant ignition or combustion.

AGD and FD are observed under a chamber pressure of 0.2–10 kPa. With only Ar in the discharge chamber, measurements in plasmas indicate that N_e increases linearly with increasing pressure at a constant net power while $T_{e\text{-}exc}$ decreases slowly. However, the ADN vapor tends to emit high-energy electrons induced by seed electrons, so $T_{e\text{-}exc}$ in FD increases instead. As pressure rises, N_e slightly increases in all discharge mediums, and the plasma also shrinks owing to the reductions in electron mean free path and ion diffusivity. In terms of energy transfer, the electron loss rate decreases while the ionization rate remains nearly the same, which also explains the increase in N_e. Furthermore, N_e decreases after ADN vapor is added mainly owing to the inelastic collisions between electrons, molecules, and water, which plays a role as an effective quencher.

We should mention that most plasmas in contact with vapors are

highly transient, so it is essential to investigate the kinetics of these plasmas. Under low-pressure discharge when the collisions are not prominent, the emission spectrum is mostly determined by plasma kinetics and production mechanisms of the excited species [31]. Chamber pressure becomes a significant parameter for discharge regime transition within a low input power range. Adding ADN-based propellant vapor into argon plasma also introduces multi-level complications. In addition, the vapor allows additional degrees of freedom for energy transfer; thus, more complex reactions are expected. This work provides not only experimental data for validating kinetic models of plasma interaction with ADN-based propellants, but guidance on improving ADN-based thruster performance with plasma-assisted ignition/combustion. As we mentioned earlier, OES with high spatio-temporal resolution should be developed to explore the kinetics of plasma interaction with an ADN-based liquid propellant. This would enable comprehensive understanding of the evolution of certain atomic and molecular species.

Funding sources

This work was supported by the National Science Foundation of China (Grant Nos. 11672359, 11872368, 11927803).

Disclosures

The authors declare no conflicts of interest.

CRediT authorship contribution statement

Fangyi Wang: Conceptualization, Methodology, Data curation, Software, Formal analysis, Investigation, Validation, Writing – original draft, Writing – review & editing. **Shaohua Zhang:** Conceptualization, Formal analysis, Supervision, Funding acquisition. **Xilong Yu:** Supervision, Project administration, Funding acquisition.

Declaration of Competing Interest

The authors declare that they have no known competing financial interests or personal relationships that could have appeared to influence the work reported in this paper.

Data availability

Data will be made available on request.

Acknowledgements

The authors acknowledge the technical assistance provided by D. H. Guo at the Institute of Mechanics, Chinese Academy of Sciences.

References

[1] H. Östmark, U. Bemm, A. Langlet, R. Sandén, N. Wingborg, The properties of ammonium dinitramide (ADN): part 1, basic properties and spectroscopic data, J. Energetic Mater. 18 (2–3) (2000) 123–138.
[2] C. Maleix, P. Chabernaud, R. Brahmi, et al., Development of catalytic materials for decomposition of ADN-based monopropellants, Acta Astronautica. 158 (2019) 407–415.
[3] A. Wada, H. Habu, Electric Ignition Characteristics of an Ammonium-Dinitramide-Based Ionic Liquid Monopropellant with Discharge Plasma, 2020.
[4] Y. Hou, Y. Yu, X. Liu, J. Chen, T. Zhang, Experimental study on microwave-assisted ignition and combustion characteristics of ADN-based liquid propellant, ACS Omega. 6 (35) (2021) 22937–22944.
[5] L. Jing, X. You, J. Huo, M. Zhu, Z. Yao, Experimental and numerical studies of ammonium dinitramide based liquid propellant combustion in space thruster, Aerosp. Sci. Technol. 69 (2017) 161–170.
[6] R. Engeln, B. Klarenaar, O. Guaitella, Foundations of optical diagnostics in low-temperature plasmas, Plasma Sources Sci. Technol. 29 (6) (2020), 063001.
[7] C.O. Laux, T. Spence, C. Kruger, Zare RJPSS, Technology, Optical diagnostics of atmospheric pressure air plasmas 12 (2) (2003) 125.
[8] B. Benstaali, P. Boubert, B. Cheron, A. Addou, Brisset JJPc, processing p, Density and rotational temperature measurements of the OH and NO radicals produced by a gliding arc in humid air 22 (4) (2002) 553–571.
[9] K. Hsieh, R. Burlica, B.R. Locke, Optical diagnostics of electrical discharge water-spray reactors for chemical synthesis 49 (1) (2012) 305–310.
[10] K.-Y. Shih, B.R. Locke, Optical and electrical diagnostics of the effects of conductivity on liquid phase electrical discharge 39 (3) (2011) 883–892.
[11] B.R. Locke, Environmental applications of electrical discharge plasma with liquid water—a mini review 6 (2012) 194–203.
[12] B. Sun, M. Sato, Clements JSJJoE., Optical study of active species produced by a pulsed streamer corona discharge in water 39 (3) (1997) 189–202.
[13] H. Akatsuka, Optical emission spectroscopic (OES) analysis for diagnostics of electron density and temperature in non-equilibrium argon plasma based on collisional-radiative model, Adv. Phys X 4 (1) (2019) 1592707.
[14] F. Wang, S. Zhang, Y. Liu, X. Yu, Instability mechanism and discharge regime diagnosis of microthrusters based on plasma properties, Appl. Opt. 60 (4) (2021) 1021–1030.
[15] F. Wang, S. Zhang, X. Yu, X. Lin, J. Li, Y. Liu, Quantitative measurement of the mixture ratio for ADN-based liquid propellants using laser-induced breakdown spectroscopy, J. Anal. At. Spectrom. 36 (9) (2021) 1996–2006.
[16] N. Shirai, H. Owada, K. Sasaki, Efficient production and transport of OH radicals in spatial afterglow of atmospheric-pressure DC glow discharge using intersecting helium flows, Plasma Sources Sci. Technol. 30 (12) (2021), 125012.
[17] H. Onishi, F. Yamazaki, Y. Hakozaki, M. Takemura, A. Nezu, H. Akatsuka, Measurement of electron temperature and density of atmospheric-pressure non-equilibrium argon plasma examined with optical emission spectroscopy, Jpn. J. Appl. Phys. 60 (2) (2021), 026002.
[18] H. Yuan, J. Feng, D.-Z. Yang, et al., Plasma characteristics and mode transition of atmospheric pressure gas–liquid discharge oxygen plasma 128 (9) (2020), 093303.
[19] P. Bruggeman, T. Verreycken, M.A. Gonzalez, et al., Optical emission spectroscopy as a diagnostic for plasmas in liquids: opportunities and pitfalls 43 (12) (2010), 124005.
[20] A. Sarani, A.Y. Nikiforov, C. Leys, Atmospheric pressure plasma jet in Ar and Ar/H2O mixtures: Optical emission spectroscopy and temperature measurements 17 (6) (2010), 063504.
[21] Trusov KJJoPDAP, Dynamics of multichannel and quasi-homogeneous sliding discharge formation in rare gases 40 (3) (2007) 786.
[22] A. Durocher-Jean, N. Delnour, L. Stafford, Influence of N2, O2, and H2 admixtures on the electron power balance and neutral gas heating in microwave Ar plasmas at atmospheric pressure, J. Phys. D. Appl. Phys. 52 (47) (2019), 475201.
[23] S. Tabaie, D. Iraji, R.J.V. Amrollahi, Measurement of electron temperature and density of atmospheric plasma needle 182 (2020), 109761.
[24] N. Ohno, M. Razzak, H. Ukai, S. Takamura, Y. Uesugi, Validity of Electron temperature measurement by using Boltzmann plot method in radio frequency inductive discharge in the atmospheric pressure range, Plasma Fusion Res 1 (2006) (28-028).
[25] Leonard RHHaSL, Plasma Diagnostic Techniques, Academic Press, New York, 1966.
[26] H.R. Griem, Plasma Spectroscopy, McGraw-Hill Book Co, 1965.
[27] M. Tahiyat, T.W. Knight, Farouk TJRoSI., Note: Plasma optical emission spectroscopy for water vapor quantification and detection during vacuum drying process 89 (11) (2018), 116108.
[28] A. Nikiforov, A. Sarani, C. Leys, The influence of water vapor content on electrical and spectral properties of an atmospheric pressure plasma jet, Plasma Sources Sci. Technol. 20 (2011), 015014.
[29] M.S. Simeni, A. Roettgen, V. Petrishchev, K. Frederickson, I.V. Adamovich, Electron density and electron temperature measurements in nanosecond pulse discharges over liquid water surface, Plasma Sources Sci. Technol. 25 (6) (2016), 064005.
[30] T. Kaneko, K. Baba, Hatakeyama RJJoAP., Static gas-liquid interfacial direct current discharge plasmas using ionic liquid cathode 105 (10) (2009), 103306.
[31] K. Inoue, S. Takahashi, N. Sakakibara, S. Toko, T. Ito, K. Terashima, Spatiotemporal optical emission spectroscopy to estimate electron density and temperature of plasmas in solution, J. Phys. D. Appl. Phys. 53 (23) (2020), 235202.